Research Article | Vol. 11, No. 10 / 1 October 2020 / Biomedical Optics Express 5586
Biomedical Optics EXPRESS

Comparison of algorithms to suppress artifacts from the natural lens in fluorescence lifetime imaging ophthalmoscopy (FLIO)

D. SCHWEITZER,[1] J. HAUEISEN,[2] J. L. BRAUER,[1] M. HAMMER,[1] AND M. KLEMM[2,*]

[1]Department of Ophthalmology, University Hospital Jena, Am Klinikum 1, 07747 Jena, Germany
[2]Institute of Biomedical Engineering and Informatics, POB 100565, 98694 Ilmenau, Germany
[*]matthias.klemm@tu-ilmenau.de

Abstract: Fluorescence lifetime imaging ophthalmoscopy (FLIO) has developed as a new diagnostic tool in ophthalmology. FLIO measurements are taken from 30° retinal fields in two spectral channels (short spectral channel (SSC): 498–560 nm, long spectral channel (LSC): 560–720 nm). Because of the layered structure of the eye, the detected signal is an interaction of the fluorescence decay of the anterior part and of the fundus. By comparing FLIO measurements before and after cataract surgery, the impact of the natural lens was proven, despite the application of a confocal laser scanning (cSLO) technique. The goal of this work was to determine the best algorithmic solution to isolate the sole fundus fluorescence lifetime from the measured signal, suppressing artifacts from the natural lens. Three principles based on a tri-exponential model were investigated: a tailfit, a layer-based approach with a temporally shifted component, and the inclusion of a separately measured fluorescence decay of the natural lens. The mean fluorescence lifetime $\tau_{m,12}$ is calculated using only the shortest and the intermediate exponential component. $\tau_{m,all}$ is calculated using all three exponential components. The results of tri-exponential tailfit after cataract surgery were considered as a reference, because the implanted artificial lens can be assumed as non-fluorescent. In SSC, the best accordance of $\tau_{m,all}$ of the reference was determined with $\tau_{m,12}$ of the tailfit before surgery. If high-quality natural lens measurements are available, the correspondence of $\tau_{m,12}$ is best with $\tau_{m,all}$ of the reference. In LSC, there is a good accordance for all models between $\tau_{m,12}$ before and after surgery. To study the pure fundus fluorescence decay in eyes with natural lenses, we advise to utilize fluorescence lifetime $\tau_{m,12}$ of a triple-exponential tailfit, as it corresponds well with the mean fluorescence lifetime $\tau_{m,all}$ of eyes with fluorescence-less artificial intraocular lenses.

1. Introduction

FLIO, a time-resolved measurement of the autofluorescence of the eye, was developed as a tool to diagnose metabolic alterations [1,2], which offered sufficient repeatability (or retest reliability) [3–5]. FLIO is based on fluorescence lifetime imaging microscopy (FLIM), which is applied to many research fields. An extensive overview about the FLIM principles and its clinical applications is given by Marcu et al. [6]. Factors having an influence on FLIO measurements, such as macular pigmentation, photoreceptor bleaching, and pupil dilation have been investigated [7–10]. For the interpretation of FLIO data, the excitation and emission spectra, as well as the fluorescence decays of endogenous fluorophores, such as NADH (reduced nicotinamide adenine dinucleotide), FAD (flavin adenine dinucleotide), lipofuscin, AGE (advanced glycation end-products), melanin, collagen, and elastin were measured and compared with data from the literature [11,12]. As these fluorophores can be located in several anatomical structures of the eye, the corresponding measurements were performed on the cornea, lens, chamber water, vitreous, and retina of porcine eyes [13,14]. The summarized fluorescence of all fluorophores in

#400059 https://doi.org/10.1364/BOE.400059
Journal © 2020 Received 11 Jun 2020; revised 8 Aug 2020; accepted 8 Aug 2020; published 15 Sep 2020

Biomedical Optics EXPRESS

all anatomical structures of the eye is detected during in vivo FLIO measurements. Based on such integral measurements, differences in fluorescence lifetimes were already detected between healthy volunteers and patients suffering from different diseases [2,15–32]. Good overviews about the physical background and the current state of clinical applications of FLIO are presented in [33,34]. FLIO has also been used in animal studies [35,36].

The eye can be considered as a structure of fluorescent layers, primarily comprised of anterior and posterior parts. The anterior part is dominated by the fluorescence of the natural lens. The posterior part consists of several retina layers, which are in FLIO often assumed as one layer because of its low depth resolution. The applied confocal detection principle is not as effective in suppressing the fluorescence signal from the anterior part [37] as it is in suppressing reflected light from the anterior part. Light is reflected on surfaces. In contrast, fluorescence is a volumetric event. Thus, the relation of the thickness of the fluorescent layers, i.e. natural lens vs. retina (4.0–4.7 mm vs. 0.2 mm), must to be taken into account.

The fluorescence of the natural lens is excited earlier in time than the fluorescence of the fundus because of the distance between them. This time-difference is visible in FLIO data, as shown in Fig. 1. Also visible in Fig. 1 is the much slower decay of the natural lens fluorescence of time in comparison to the fundus. The fluorescence lifetime of the natural lens is in the order of a few nanoseconds, while the fluorescence lifetimes of the fundus are mostly less than one nanosecond (in the fovea even less than 100 ps). Thus, the superposition of the fluorescence lifetimes from fundus and natural lens causes an elongation of the measured fluorescence lifetime compared to the pure fluorescence lifetime of the fundus.

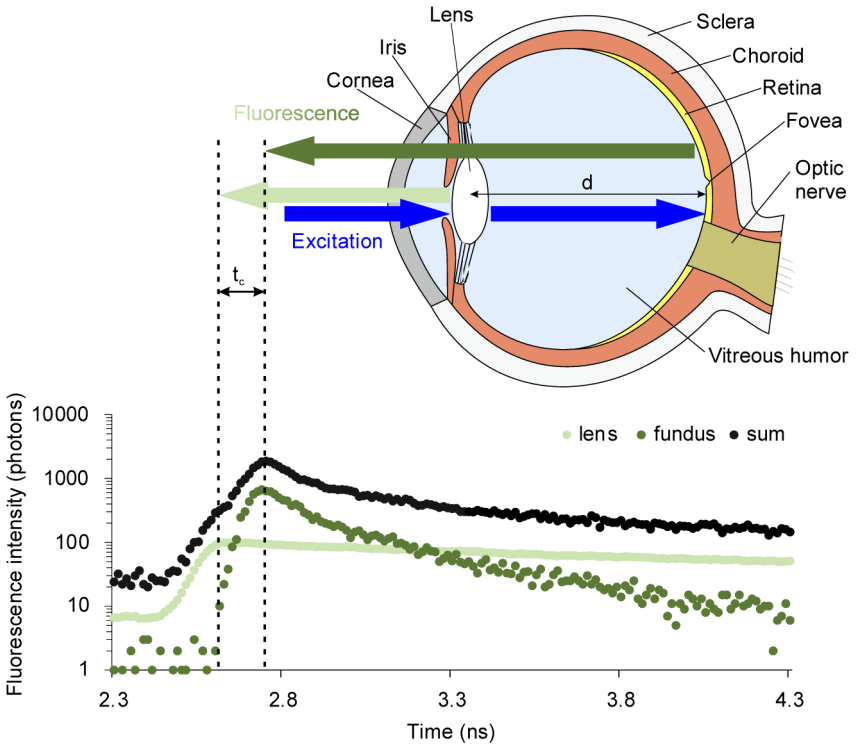

Fig. 1. Top: Schema of the human eye. Bottom: Sections of time-resolved fluorescence decays of the natural lens (light green), the fundus (dark green) and their superposition (black), which is the measured signal of a single pixel in FLIO.

Biomedical Optics EXPRESS

Figure 2 shows the fluorescence spectrum of a natural lens, which was measured by a confocal laser scanner ophthalmoscope (cSLO) connected to a spectrograph [38].

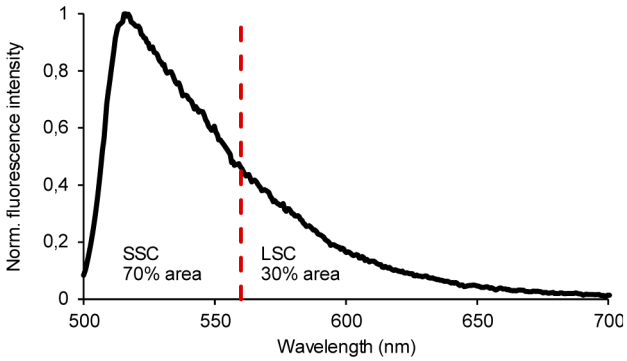

Fig. 2. In vivo measured fluorescence spectrum of the crystalline lens of a 62-year-old man above 500 nm, excited at 468 nm. The dashed line represents the cut-off wavelength for both spectral channels of the FLIO device. SSC: short spectral channel; LSC: long spectral channel.

The emission spectrum of the natural lens is predominantly in FLIO's short spectral channel. The fluorescence emissions of several expected fundus fluorophores (e.g. FAD, AGE (e.g. pentosidine, argpyrimidine), collagen, elastin, etc.) are mostly in the short spectral channel, [39], while the emission of e.g. A2E (N-retinylidene-N-retinylethanolamine, the component VIII of lipofuscin, maximum at 600 nm) is in the long spectral channel.

Hence, the fluorescence of the natural lens is considered an artifact which lowers the signal-to-noise ratio of the fundus fluorescence, possibly decreasing FLIO's sensitivity as a diagnostic tool for retinal diseases.

Intraocular lenses (IOL) are an artificial replacement for the natural lens, mostly used in therapy of strong cataract, and do not emit a considerable fluorescence signal. Consequently, FLIO measurements in patients with IOL do not suffer from artifacts caused by the natural lens fluorescence and contain only fluorescence signal from the fundus. Since FLIO should also work well in patients with natural lenses, the artifacts in FLIO data caused by the natural lens fluorescence have to be suppressed. As mentioned above, the confocal detection principle is not able to suppress the natural lens sufficiently and hardware modification of the FLIO device to solve this problem, e.g. [40], are currently not possible. In principle, the suppression of the disturbing fluorescent layer, located in front of the fluorescent layer of interest, is possible by multi-photon excitation. The required high exposure could damage the retina. According to Wang [41], there is only a factor of two in two-photon excitation between a fluorescence signal strong enough for imaging and damaging the retina. Despite this limitation, Hunter et al. [42] described the successful application of two-photon excitation in combination with adaptive optics for the detection of the pure fundus fluorescence in monkey eyes. The separation of the fluorescence of a single layer in a layered structure by combination of OCT and fluorescence is the goal of current research. Several approaches are described for the combination of OCT and fluorescence measurement in endoscopic applications [43,44]. The results are 3D OCT images but only 2D surface fluorescence images. Thus, the natural lens fluorescence in FLIO should be suppressed by means of software algorithms, which is the aim of this work. Therefore, FLIO measurements from patients with IOL will serve as the artifact free reference and FLIO measurements of the same patients from before the IOL insertion (cataract surgery) will be used as data basis to evaluate different algorithmic approaches to suppress the natural lens fluorescence.

Biomedical Optics EXPRESS

A recommendation is given as to how FLIO measurements should be compared between healthy volunteers and patients.

2. Material and method

2.1. Instrumentation

Time-resolved measurements were performed using the fourth version of a FLIO confocal laser scanning ophthalmoscope (cSLO), which was constructed by Heidelberg Engineering GmbH (Heidelberg, Germany) [4], according to their experiences with previous versions developed at the University eye clinic Jena.

In short, the basic device is a confocal laser scanning ophthalmoscope (cSLO, HRA-2, Heidelberg Engineering GmbH) using the SPECTRALIS system, an expandable diagnostic imaging platform that combines scanning laser fundus imaging with high-resolution optical coherence tomography (OCT). A picosecond pulsed diode laser excites the endogenous fluorescence at 473 nm (BDL-473-SMC, Becker & Hickl GmbH, Berlin, Germany) with a repetition rate of 80 MHz. The fluorescence decay is detected by time correlated single photon counting (TCSPC) from a 30-degree fundus field. The time resolution is 12.2 ps, the image repetition rate is 8.8 frames per second and the image size is 256×256 pixels.

Fluorescence decay is detected in a short spectral channel (SSC: 498 nm - 560 nm) and in a long spectral channel (LSC: 560 nm - 720 nm). The fluorescence is detected by a hybrid detector (HPM-100-40, Becker & Hickl GmbH), connected with a TCSPC board (SPC 150, Becker & Hickl GmbH) in each channel. For compensation of eye movements, infrared reflection images are recorded in parallel to the fluorescence images.

By combining the cSLO and the TCSPC technique [45,46] with multiple detectors, FLIO generates time-, space-, and spectrum-resolved fluorescence decay data sets. It takes approximately two minutes for each FLIO measurement to reach the target of 1000 photons per pixel [4] in the macular region in the SSC. Details of the FLIO device are described elsewhere [4,7,47].

2.2. Participants

The FLIO data were measured in 31 patients before and after cataract surgery (17 males and 14 females). All patients underwent a detailed clinical ophthalmic examination, including funduscopy, slit-lamp examination, and intraocular pressure measurement. All patients were diagnosed with cataracta provecta (advanced cataracts). Three patients were excluded because of an extremely dense natural lens. The age range was 49 to 88 years with a mean of 72.6 ± 9.1 years. The pupil was dilated using tropicamide and phenylephrine HCl. All measurements were taken one day before cataract surgery and one month after surgery. Before cataract surgery, the fluorescence decay of the natural lens was measured separately.

The study was performed according to the tenets of the declaration of Helsinki and approved by the ethic committee of the University Hospital Jena. Written informed consent was obtained from all patients prior to study participation.

2.3. Data analysis

To improve the signal-to-noise ratio, spatial binning with a factor of 2 (5×5 pixels) was applied to the FLIO data before the following basic model functions were applied:

Multi-exponential model:

$$\frac{I_1(t)}{I_0} = IRF * \sum_i \alpha_i \cdot e^{-\frac{t}{\tau_i}} + b \tag{1}$$

With I - fluorescence intensity, IRF - instrumental response function, α_i - amplitude, τ_i - fluorescence lifetime, and b - background (offset). The background is fixed to 0.1 photons per

Biomedical Optics EXPRESS

pixel after binning, which was experimentally determined for typical acquisition times in the dark room, where all FLIO measurements were conducted. In this paper, a tri- and four-exponential fit is used ($i = 3$ and $i = 4$).

Layer-based approach with temporally shifted component:

$$\frac{I_1(t)}{I_0} = IRF * \sum_i \alpha_i \cdot e^{-\frac{t-tc_i}{\tau_i}} + b \tag{2}$$

with tc_i - time shift of the exponential component i.

Lens-corrected approach:

$$\frac{I_1(t)}{I_0} = IRF * \sum_i \alpha_i \cdot e^{-\frac{t-tc_i}{\tau_i}} + \alpha_{lens} \cdot I_{lens}(t - tc_{lens}) + b \tag{3}$$

with $I_{lens}(t\text{-}tc_{lens})$ - fluorescence intensity of the lens, time shifted by tc_{lens}, α_{lens} - amplitude of the lens fluorescence.

The Eq. (1), (2), and (3) use in different manner specific conditions of the fluorescence lifetime measurement at the eye to isolate the pure fluorescence of the retina. The models according to Eq. (1) consider the multi-exponential approximation, which is commonly used in FLIM. The models according to Eq. (2) use the specific information that the fluorescence signal of the natural lens appears earlier at the detector than the retinal fluorescence signal to separate of both signals. The models according to Eq. (3) use the separately measured fluorescence of the natural lens to compensate its contribution in the detected sum fluorescence signal of the eye, ideally resulting in the pure retinal fluorescence signal.

Fluorescence measurements in two spectral channels permit to a certain degree the discrimination of endogenous fluorophores according to their emission spectra. According to Fig. 2, the impact of the fluorescence of the natural lens should be different in both spectral channels.

For the reference, it is assumed that the artificial lens emits no fluorescence and the impact of the fluorescence of the cornea is assumed to be negligible. Thus, there is no influence of the slow fluorescence decay from the natural lens and the fluorescence lifetimes are solely related to the fundus. Despite the lack of natural lens fluorescence, a multi-exponential model (Eq. 1) with three exponential components is required to model the reference data to achieve the best curve of residuals and the lowest χ^2 error (reduced form):

$$\chi_r^2 = \frac{1}{m - \mathrm{p}} \cdot \sum_{j=1}^{m} \frac{(I_M(t_j) - I_C(t_j))^2}{I_M(t_j)} \tag{4}$$

where m is the number of time channels of the photon histogram, $I_M(t_j)$ is the number of measured photons, $I_c(t_j)$ is the number of calculated photons estimated using Eq. (1), (2) or (3), and p is the number of free parameters in the model.

The model for the reference is applied in a tailfit manner, which means that only the decay of the fluorescence signal is used.

In the measurements taken before the cataract surgery, the fluorescence signal from the fundus is superimposed by the fluorescence signal of the natural lens. Nine different models (M1–M9) are applied to the measurements to minimize the impact of the natural lens fluorescence and to extract only the fundus fluorescence signal, as listed in Table 1.

Model M1 is identical to the reference, except that only measurements from before the cataract surgery are employed. M1 reflects the way data analysis is done in most clinical FLIO studies thus far. For M2, both the rising slope and the decay of the fluorescence are used to fit the model to the measured data. Otherwise, M2 is identical to M1.

The fluorescence of the natural lens causes a stepped slope in the measured fluorescence signal, which cannot be modelled with Eq. (1). Therefore, a layer-based approach (Eq. 2) is applied

Biomedical Optics EXPRESS

Table 1. Applied models and their parameters

Label	Before / After Surgery	# Exp. Functions	Eq.	Temporally Shifted Exponent	Used Time Points	Natural Lens Measurement
Reference	after	3	1	n/a	tailfit	n/a
M1	before	3	1	n/a	tailfit	n/a
M2	before	3	1	n/a	all time points	n/a
M3	before	3	2	exp. 3: variable	all time points	n/a
M4	before	3	2	exp. 3:172 ps fix	all time points	n/a
M5	before	4	2	exp. 4: variable	all time points	n/a
M6	before	3	3	n/a	all time points	all utilized
M7	before	3	3	exp. 3: variable	all time points	all utilized
M8	before	3	3	n/a	all time points	high-quality
M9	before	3	3	exp. 3: variable	all time points	high-quality

in M3, M4, and M5. In M3, the temporal shift tc_3 for the longest component, representing the fluorescence signal of the natural lens, is variable and adapted to the data of each patient. For M4, the temporal shift tc_3 is fixed to 172 ps, which corresponds to the distance of 18.9 mm between the natural lens and fundus of Gullstrand's normal eye, using a refractive index $n = 1.3668$ for the vitreous:

$$tc = \frac{2 \cdot d \cdot n}{c} \tag{5}$$

with d - distance between the fluorescent layers, c – the speed of light.

As the temporally shifted exponential component represents the natural lens fluorescence, only two exponential components would remain to model the fundus fluorescence signal in M3 and M4. Thus, M5 employs four exponential components: three exponential components to model the fundus fluorescence and the fourth exponential is temporally shifted to model the natural lens fluorescence.

A separately taken measurement of the natural lens was included in the modelling for M6 in addition to three exponential components (Eq. 3). For M7, the longest exponential component was temporally shifted by tc_3 to model residual fluorescence signals of the eye's anterior part, in addition to the measured fluorescence signal of the natural lens.

M8 uses the same equation as M6, but only high-quality natural lens measurements are utilized. Similarly, M9 corresponds to M7, and only the high-quality natural lens measurements are utilized. The reasoning behind M8 and M9 is the difficulty for the FLIO operator to find the correct focal point for a natural lens without any visible structure. Thus, only 11 measurements of the natural lens were high-quality, which means that the rising edge of its fluorescence signal is not stepped, but steep, and the decay part of the signal does not contain any sections with a rising signal. M8 and M9 demonstrate the potential to minimize the impact of the fluorescence decay of the natural lens, if the fluorescence of the natural lens is detected with high quality.

For comparison of the models, the following mean fluorescence lifetimes were calculated:

$$\tau_m = \frac{\sum_i \alpha_i \cdot \tau_i}{\sum_i \alpha_i} \tag{6}$$

$\tau_{m,1,2}$ Only the shortest (τ_1) and the intermediate (τ_2) fluorescence lifetime and their corresponding amplitudes (α_1, α_2) are considered.

$\tau_{m,\,all}$ All fluorescence lifetimes and corresponding amplitudes are considered.

Measurements in different areas consider different distributions of fluorophores at the fundus. A standardized early treatment diabetic retinopathy study (ETDRS) grid, centered at the macula

Biomedical Optics EXPRESS

[48], was placed by an expert in each FLIO measurement. Its central area (C), as well as the inner ring (IR), and the outer ring (OR), were used for further analyses (see Fig. 3). For each region (C, IR, and OR) from each measurement, the mean values of the fluorescence lifetimes were used for further statistical evaluation. As not all data followed a normal distribution (Shapiro-Wilk test [49]), the non-parametric Wilcoxon signed-rank test was used to compare M1 to M7 against the reference, and the Wilcoxon rank-sum test was used for the comparison of M8 and M9 against the reference.

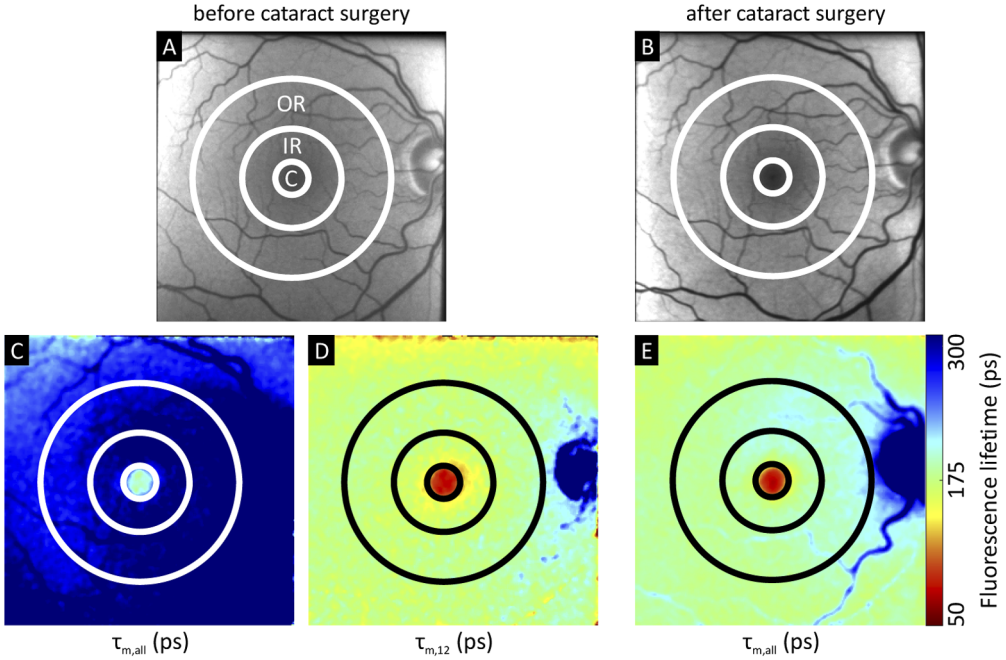

Fig. 3. Fluorescence intensity (A and B) and fluorescence lifetimes (C, D, and E) before cataract surgery (A, C, and D), and after cataract surgery (B and E). C (M1) and E (Reference) show the mean fluorescence lifetime $\tau_{m,all}$ using three exponential components while D (M1) shows $\tau_{m,12}$ using only the first two exponential components. There is a good correspondence between $\tau_{m,all}$ after cataract surgery with $\tau_{m,12}$ before cataract surgery. The color scaling is identical for all fluorescence lifetimes.

The FLIMX [50] software package was used to determine and analyze the fluorescence lifetime in the time-resolved fluorescence data, which is documented and freely available for download under the open source BSD–license (http://www.flimx.de).

3. Results

Figure 3 shows images of fundus autofluorescence in SSC obtained with the FLIO device before and four weeks after cataract surgery with lens replacement. The preoperative fluorescence intensity image shows remarkably lower contrast than the image recorded after surgery. This can be attributed to the strong autofluorescence of the natural lens upon excitation at 473 nm [51]. In addition, a large difference of the mean fluorescence lifetime $\tau_{m,all}$ before cataract surgery in comparison to after cataract surgery is visible, while the mean fluorescence lifetime $\tau_{m,12}$ from before cataract surgery is very similar to the mean fluorescence lifetime $\tau_{m,all}$ after surgery. This excellent correspondence between $\tau_{m,all}$ after surgery with $\tau_{m,12}$ before surgery, which corresponds to the retinal fluorescence, was achieved best by M1.

Biomedical Optics EXPRESS

The detailed fluorescence lifetimes $\tau_{m,all}$ and $\tau_{m,12}$ of the considered locations in SSC and LSC are given for each model shown in Fig. 4.

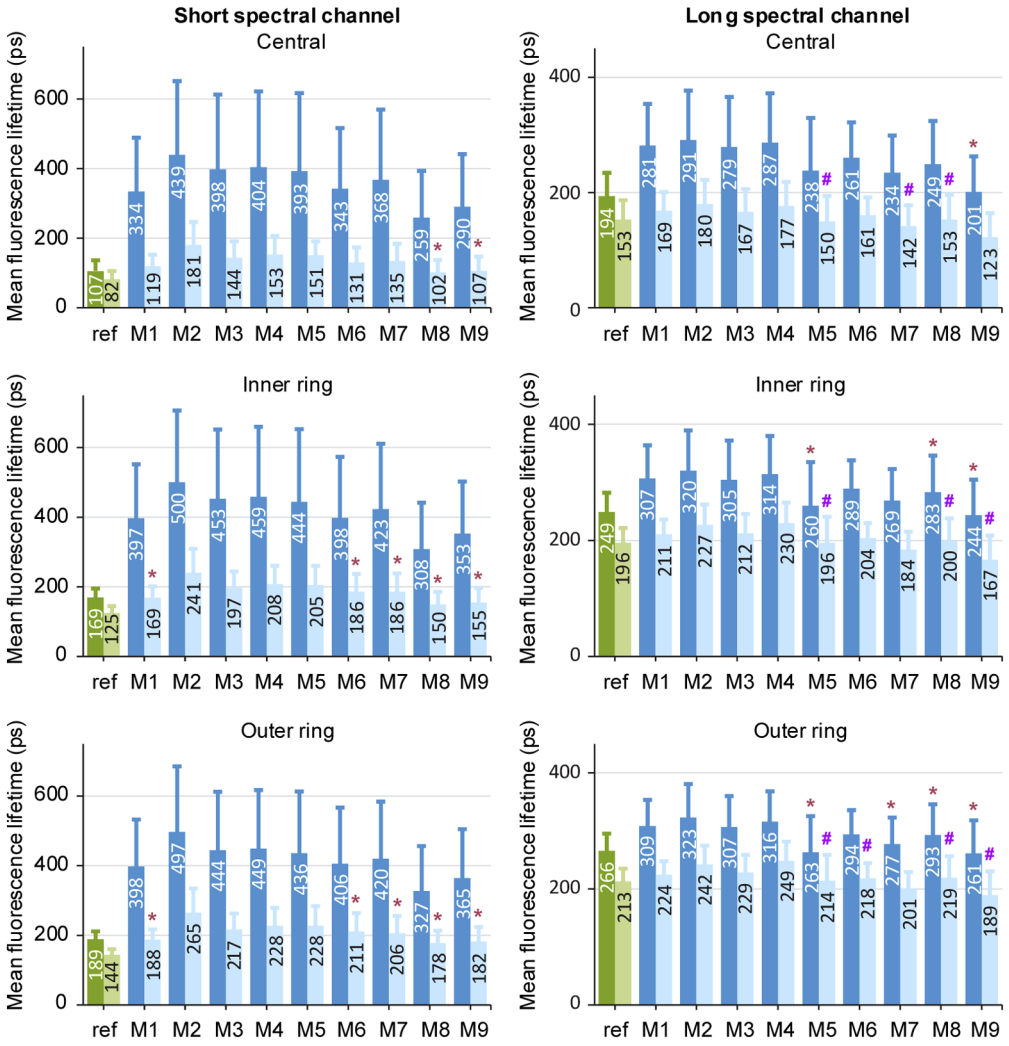

Fig. 4. Mean fluorescence lifetimes $\tau_{m,all}$ (dark color) and $\tau_{m,12}$ (light color) including standard deviation averaged over all patients for the reference (green) and all models (blue) for both spectral channels and all regions. Red * indicate **no** significant difference to $\tau_{m,all}$ of the reference and purple # indicate **no** significant difference to $\tau_{m,12}$ of the reference.

The fluorescence lifetime depends, to a certain degree, on the location at the fundus. As shown in Fig. 4 (green bars), the mean fluorescence lifetimes $\tau_{m,all}$ after surgery are shortest in the central area of the ETDRS grid and are longest in the outer ring. This behavior is valid in both spectral channels. This clear local difference of $\tau_{m,all}$ is reduced before surgery because the long fluorescence decay of the natural lens overlays the fundus fluorescence decay.

Statistical tests were applied to determine non-significant median differences ($p > 0.05$) between $\tau_{m,12}$ of all models and $\tau_{m,all}$ of the reference for SSC (Fig. 4, left side, red *). A good correspondence between measurements after surgery and measurements before surgery exists for M1 (three-exponential tailfit), M6 (three-exponential fit with additional natural lens measurement), as well as for M7 (three-exponential fit with shifted tc_3 and additional natural

Biomedical Optics EXPRESS

lens measurement) in the inner and the outer ring. The utilization of high-quality natural lens measurements in M8 and M9 resulted in good correspondence of their $\tau_{m,12}$ with $\tau_{m,all}$ of the reference for all regions. For LSC, the median differences between $\tau_{m,all}$ of all models and $\tau_{m,all}$ of the reference (Fig. 4, right side, red *) were tested. The null-hypothesis was accepted for M5 und M8 in the inner ring and the outer ring. For M9, the distributions of $\tau_{m,all}$ were comparable with $\tau_{m,all}$ of the reference in all locations. In addition, the median differences between $\tau_{m,12}$ of all models and $\tau_{m,12}$ of the reference (Fig. 4, purple #) were tested in LSC. In the outer ring, a good agreement was found in M5, M8, and M9 and partly for M6 and M7.

The largest deviations between reference and M1-M9 for both $\tau_{m,12}$ and $\tau_{m,all}$ were found in the central area in SSC and LSC. The smallest differences were found in the outer ring.

Results for the figure of merit (Eq. 4), the calculated tc_i values and the estimated fractional fluorescence of the natural lens are listed in Tables S1 and S2 in Supplement 1.

To reduce the complexity, the data shown in Fig. 5, 6 and 7 is restricted to the outer ring. Figure 5 depicts $\tau_{m,all}$ in the outer ring from both spectral channels in more detail. In SSC, $\tau_{m,all}$ of the tri-exponential model M2, which uses the entire fluorescence time range, is reduced from 497 ps before surgery to 199 ps after surgery (data not shown). M2's fluorescence lifetime $\tau_{m,all}$ is 163% longer than the reference (tailfit after surgery). This is the largest deviation from the reference of all models. In M8 and M9, which use high-quality lens measurements in addition to the tri-exponential fit, the deviation of $\tau_{m,all}$ from reference is reduced to 73%. In LSC, the deviations of $\tau_{m,all}$ from the reference in all models and in all regions are considerably smaller than in SSC (Fig. 4). In the outer ring, the deviation from the reference is largest for $\tau_{m,all}$ in M2 (21%), but much smaller than in SSC. $\tau_{m,all}$ of M1 is 16% longer than in the reference. Nearly the same result as in the reference was obtained in M5 (-1%, four-exponential fit with variable *tc4*) and in M9 (-2%, tri-exponential fit with variable *tc3* and high-quality lens measurements). In M8, $\tau_{m,all}$ in LSC is 10% longer than the reference.

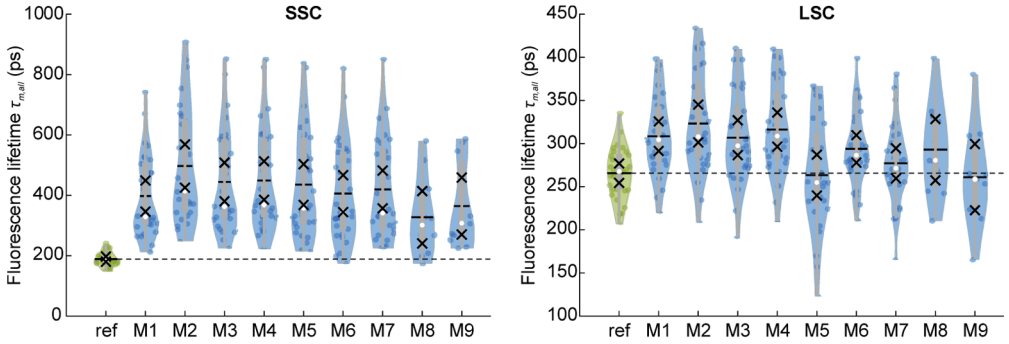

Fig. 5. Violin diagrams of $\tau_{m,all}$ for reference (green) and all models (blue) in the outer ring of the ETDRS grid. The white dot represents the median, the black line represents the mean, and the black crosses represent the 95% confidence interval.

The difference of $\tau_{m,12}$ in eyes with natural lens and $\tau_{m,all}$ in eyes with artificial intra-ocular lenses is quite small for all models in SSC (Fig. 6). Especially in M1, this difference is only -0.5%. This is an important result because most FLIO measurements have been evaluated using M1 so far. In M6 and M7, $\tau_{m,12}$ was longer by only 12% and 9% respectively than $\tau_{m,all}$ of the reference. In M3 (variable tc_3), the difference was only 15%. In case of a fixed tc_3 at 172 ps (M4), the difference was 20% (25% for $tc_3 = 140$ ps, data not shown).

The fundus fluorescence decay in SSC without the impact of the long fluorescence decay of the natural lens can be estimated, if the fluorescence lifetime $\tau_{m,12}$ is calculated in measurements before surgery. Figure 6 shows pairwise differences of the fluorescence lifetime $\tau_{m,12}$ from before

Biomedical Optics EXPRESS

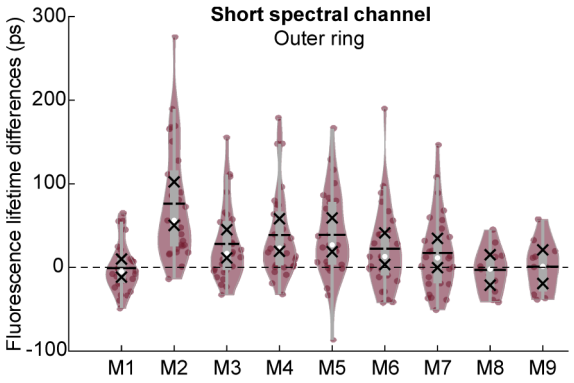

Fig. 6. Pairwise differences of $\tau_{m,12}$ from all models and $\tau_{m,all}$ from reference for the outer ring. The white dot represents the median, the black line represents the mean, and the black crosses represent the 95% confidence interval.

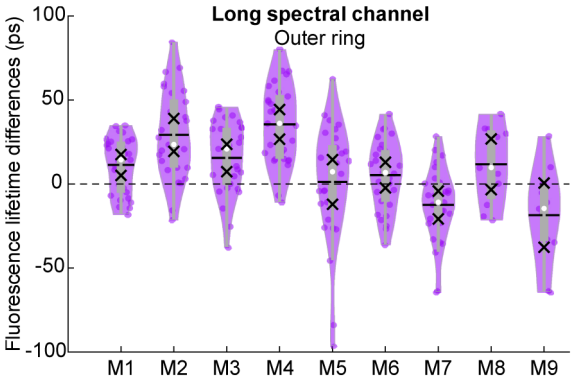

Fig. 7. Pairwise differences of $\tau_{m,12}$ of all models and $\tau_{m,12}$ of the reference in LSC. The white dot represents the median, the black line represents the mean, the black crosses represent the 95% confidence interval.

surgery (M1 – M9) and $\tau_{m,all}$ from after surgery (reference) in SSC, as recommended by the CONSORT Group [52].

The pairwise differences shown in Fig. 6 provide more information than Fig. 4 by eliminating the influence of patient-specific fluorescence lifetime alterations, e.g. a longer fluorescence lifetime due to age. Thus, only the deviations caused by each model remain. A negative pairwise difference means, that the model estimated a shorter fluorescence lifetime than the reference (and vice versa for positive differences). The pairwise difference for M1, M8 and M9 possess a nearly ideal shape with a mean value of almost zero. The remaining models are biased towards positive pairwise differences, estimating longer fluorescence lifetimes than the reference.

Similar to Fig. 6, Fig. 7 shows pairwise differences of the fluorescence lifetime $\tau_{m,12}$ from before surgery (M1 – M9) and $\tau_{m,12}$ from after surgery (reference) in LSC.

There is a good correspondence for $\tau_{m,12}$ before and after cataract surgery in LSC. A difference below 8% was calculated in M1, M3, M5, M6, M7, and M8. The largest difference of 17% was determined in M4. Even in M2, the model with the largest difference in SSC, the difference to $\tau_{m,12}$ of the reference was only 14% in LSC.

Biomedical Optics EXPRESS

4. Discussion

4.1. Summary

The fluorescence lifetime imaging ophthalmoscopy technique is in the process of evolving from prototype technology to clinical application. Part of this process is the identification and characterization of artifacts in the measured FLIO data and their suppression. This work describes the fluorescence of the natural lens as a noteworthy artifact in FLIO and how the effect of this artifact can be reduced by means of data processing. Therefore, FLIO data of 29 patients has been acquired before and after the replacement of the natural lens with a non-fluorescent artificial lens. By using the FLIO data after the surgery as artifact-free reference, the authors could evaluate 9 different models (based on three different algorithms) to analyze the FLIO data from before the surgery in combination with two different variants of a mean fluorescence lifetime. In SSC, $\tau_{m,12}$ of all models was generally much closer to $\tau_{m,all}$ of the reference in comparison to each model's $\tau_{m,all}$. The mean fluorescence lifetime $\tau_{m,12}$ utilizing only the short and the intermediate fluorescence lifetime of M8 and M9, both tri-exponential models with an additionally included separately measured fluorescence signal of the natural lens of high quality, achieved the lowest deviations to the tri-exponential fluorescence lifetime $\tau_{m,all}$ of reference in FLIO's short spectral channel in all regions. M1, a tri-exponential model, which is only applied to the decay of the fluorescence signal (tailfit) achieved even lower deviations to $\tau_{m,all}$ of the reference in the inner and the outer ring of the short spectral channel. In the long spectral channel, $\tau_{m,all}$ of M9 could match $\tau_{m,all}$ of reference in all investigated regions while $\tau_{m,12}$ of M5 and M8 had the lowest deviations to $\tau_{m,12}$ of the reference. The authors recommend $\tau_{m,12}$ of M1 in SSC and $\tau_{m,12}$ of M5 in LSC because both models don't require a separate measurement of the patient's natural lens reducing FLIO's stress for the patient.

4.2. Fluorescence of the natural lens in FLIO

The eye has a structure of fluorescent layers: anterior and the posterior parts. The fluorescence of the natural lens dominates the fluorescence of the anterior part. The posterior part consists of several fundus layers, which are assumed as only one layer in FLIO because of insufficient depth resolution.

As demonstrated in Fig. 1, the fluorescence decay of the natural lens overlays the fundus fluorescence. Patients suffering from retinal diseases are predominantly of advanced age. The fluorescence of the natural lens increases with age, especially related to cataract formation. Thus, the artifacts caused by the fluorescence of the natural lens are most prominent in FLIO's typical patients. The mean fluorescence lifetime (bi-exponential fit) of the natural lens from a porcine eye is 1120 ps [11]. This value can be used for orientation, because the anatomical structure of a porcine eye is comparable to a human eye.

Independent of a bi- or tri-exponential approximation of the fluorescence lifetime in FLIO data, only prolongations of the mean fluorescence lifetime have been found in all clinical studies of patients and healthy volunteers with a natural lens so far [33,34]. Thus, it is possible that these prolongations of the fluorescence lifetime are influenced to a certain degree by the fluorescence lifetime of the natural lens. For example, comparing FLIO measurements of diabetic patients and healthy volunteers, considerable elongation of the fluorescence lifetime was found in diabetic patients [53]. Both groups had only eyes with natural lenses. In contrast, the difference in fluorescence lifetime was much smaller, when only patients and volunteers with artificial lenses were analyzed (6 participants per group). Karumanchi et al. [54] showed that diabetic patients and healthy volunteers can be discriminated according to fluorescence changes of the natural lens. Thus, it cannot be excluded that the prolongation of the fluorescence lifetime in diabetic patients found in FLIO data [18,19] may be caused to a certain degree by the fluorescence of the natural lens.

Biomedical Optics EXPRESS

4.3. Comparison tri-exponential fits before and after surgery (ref, M1, M2)

The fluorescence decay after surgery is well fitted by $\tau_{m,all}$ with a tri-exponential tailfit, which can also be seen in the fluorescence lifetimes of the reference: $\tau_{m,all}$ is longer than $\tau_{m,12}$ in all regions. This means, beside the short fluorescence lifetime of the pigment epithelium and the neuronal retina [13], the longer fluorescence lifetimes of connective tissue, such as collagen and elastin [11,13], contribute to the fundus fluorescence decay.

The considerable impact of long fluorescence decay of the natural lens was demonstrated by the tri-exponential fit of the entire fluorescence time range (M2) before and after cataract surgery. The mean fluorescence lifetime $\tau_{m,all}$ in SSC decreased from 497 ps before surgery down to 199 ps after cataract surgery (outer ring), which confirms the impact of fluorescence decay of the natural lens for subjects in an extended range of age.

A certain suppression of the natural lens fluorescence can be achieved by tailfit approximation (M1) in comparison to M2. In this case, $\tau_{m,all}$ is reduced from 497 ps in M2 to 398 ps in M1 (SSC, outer ring).

Interestingly, the means and medians of the fluorescence lifetime $\tau_{m,12}$ of the fluorescence decay in M1 are nearly identical with the fluorescence lifetime $\tau_{m,all}$ after cataract surgery. The mean value of $\tau_{m,12}$ of all patients in the outer ring in SSC is only 0.5% shorter than $\tau_{m,all}$ of the reference. Thus, the fluorescence lifetime τ_3 in M1 corresponds to the fluorescence decay of the natural lens. This correspondence between $\tau_{m,all}$ of the reference and $\tau_{m,12}$ before surgery was best for M1 in comparison with all other models in the outer ring. From this result, it can be advised that $\tau_{m,12}$ in tri-exponential tailfit (M1) should be used for the comparison of the fundus fluorescence decay in healthy volunteers with other types of patients, with natural lenses. It should be mentioned that the patients in this study were suffering from cataracts only. Fundus diseases can deteriorate this accordance.

It was noted that $\tau_{m,12}$ increased in the ETDRS grid from the central area to the outer ring in both spectral channels, independent of the applied model. This confirms the results by Dylsi et al. [4], although they approximated the fluorescence decay only by a bi-exponential tailfit. The reason for the increasing $\tau_{m,12}$ might be an increased thickness of the neuronal retina. In SSC, an additional influence of the short fluorescence lifetime of the macular pigment xanthophyll can be assumed [7,8].

The lower effect of fluorescence decay of the natural lens in LSC compared to SSC was demonstrated by the difference of $\tau_{m,all}$ before surgery (M1 through M9) and after surgery (reference). Whereas, in SSC, the difference was between 110% and 212%, in LSC the difference was considerably smaller, with a range of 16% to 45%, depending upon the location in the ETDRS grid. The differences for $\tau_{m,12}$ at the central area, and inner and outer rings between M1 and the reference were determined as 45%, 35%, and 30% in SSC, but as only 10%, 8%, and 5% in LSC.

4.4. Layer-based approach (M3, M4, M5)

The contribution of the layered structure of the eye on the decay of fluorescence in FLIO data was investigated in [50,55–57]. The fluorescence signal of the natural lens appears by the time tc_i earlier on the detector than the fundus fluorescence (Eq. 5). Both the excitation light and the fundus fluorescence light travel the distance between the natural lens and the fundus. This results in a shoulder of the rising edge of the fluorescence signal (Fig. 1). The visibility of this shoulder depends on the full width at half maximum (FWHM) of the instrument response function (IRF). This shoulder is clearly visible when using the ultra-fast hybrid detector HPM-100-06 (Becker & Hickl GmbH), which has an IRF of 40 ps (FWHM) after convolution with the laser pulse [56]. The shoulder was also visible using the microchannel plate photomultiplier tube R3809U-50 (Hamamatsu Photonics Europe GmbH, Herrsching am Ammersee, Germany) with an IRF of 80 ps (FWHM) in an earlier version of the FLIO device [57]. The current FLIO device utilizes

Biomedical Optics EXPRESS

GaAsP hybrid detectors (HPM-100-40, Becker & Hickl GmbH). This detector has a higher sensitivity than the microchannel plate photomultiplier and the ultra-fast hybrid detector, but the IRF is 120 ps (FWHM) [50]. Using the HPM-100-40 detector, the shoulder is only weakly visible. It seems that the product of sensitivity and dynamic behavior might be a constant for each detector type.

It might be possible to calculate a rough estimation of the distance between natural lens and fundus with FLIO's current time resolution using tc_i from Eq. (2) and Eq. (5). The separation of the fluorescence from several fundus layers is the goal of current research. Therefore, the principle of time-shifted fluorescence measurement was investigated by Gräfe et al. [58]. In their experiments using a femtosecond pulse laser, a depth resolution of 100 µm was achieved by time gating and optical parametric amplification.

In M3, the time shift tc_3 of the third exponential component, which corresponds to the fluorescence decay of the natural lens, was assumed as a free parameter. The difference between $\tau_{m,all}$ in tailfit after surgery (reference) to $\tau_{m,12}$ of M3 was 15% in the outer ring. In M4, with fixed $tc_3 = 172$ ps, this difference was 21%. The same difference was also calculated for $tc_3 = 140$ ps (data not shown). This comparatively large difference is in contrast to the results by Becker et al. [56]. Similar to M4, they also used a tri-exponential model with τ_3 shifted by a fixed tc_3. They found a good correspondence between $\tau_{m,all}$ after surgery $\tau_{m,12}$ before cataract surgery. Also, the shoulder in the rising edge was very well fitted. They noted comparable results with fixed tc_3 between 130 ps and 150 ps. There are some possible reasons for the different results in [56] compared to this work. Becker et al. used an ultra-fast hybrid detector for their measurements. A very short synthetic IRF instead of a measured IRF was applied in the modelling procedure. Thus, a better time resolution was possible. In addition, no ETDRS grid was applied. Instead, the entire fluorescence lifetime image was used for the analysis. Further, it is not clear how many patients were investigated.

In M5 (the fourth exponential component is temporally shifted by tc_4, the parameter is not fixed) a good correspondence was found in SSC between $\tau_{m,12}$ and $\tau_{m,all}$ of reference in the central area. There were also only small deviations between M5's $\tau_{m,all}$ and $\tau_{m,all}$ of the reference for the inner ring and the outer ring in LSC. The correspondence between M5's $\tau_{m,12}$ and $\tau_{m,12}$ of the reference was very good for all regions. As described in methods, $\tau_{m,12}$ in M5 is calculated from the first three exponential components. Thus, it seems that the fourth exponential is able to model the weak fluorescence decay of the natural lens in LSC.

In the layer-based approach, the differences of the fluorescence lifetimes between before surgery and after surgery were smaller, when tc_i was a free parameter and not fixed. The free tc_i parameter allowed for a patient-individual adaptation, which seemed beneficial.

The application of the layer-based approach resulted in an inferior agreement of $\tau_{m,12}$ before surgery and $\tau_{m,all}$ after surgery (reference) compared to the application of the simpler tri-exponential tailfit (M1). This result is only valid for the used FLIO hardware configuration. If detectors with a narrower IRF are used, a better correspondence between $\tau_{m,all}$ after surgery and $\tau_{m,12}$ before surgery can be expected.

4.5. Fits with additional fluorescence of the natural lens (M6, M7, M8, M9)

The authors initially expected that models, which use an additional decay measurement of the natural lens would be best suited to estimate the fundus fluorescence decay after cataract surgery from data before the surgery. However, this was not always the case in this study.

Specifically, M6 and M7 (all natural lens measurements) yielded generally worse results when compared to M8 and M9 (high-quality natural lens measurements only). The measurement of the natural lens fluorescence decay is quite difficult because the operator has to focus correctly at the structure-less lens, and no standardization exists for this procedure. Furthermore, the

Biomedical Optics EXPRESS

complexity of the modelling is increased because of the inclusion of the single curve natural lens fluorescence decay.

As described above, the effect of the natural lens fluorescence is stronger in SSC compared to LSC. That can even be seen when utilizing the separate all natural lens measurements. In the outer ring of M6 (LSC), $\tau_{m,all}$ before surgery is only 10% longer than $\tau_{m,all}$ after surgery and the deviation of $\tau_{m,12}$ from $\tau_{m,12}$ of the reference is only 2%.

As shown in Fig. 4, there is an excellent accordance between $\tau_{m,12}$ in M8 and M9 with $\tau_{m,all}$ of the reference in the inner and outer rings in SSC. In LSC, $\tau_{m,all}$ of M9 corresponds well with $\tau_{m,all}$ of the reference in all regions, while $\tau_{m,12}$ of M8 corresponds well with $\tau_{m,12}$ of the reference in all regions.

In comparison to models using a layer-based approach (Eq. (2); M3, M4, M5), an improved adaption of the rising edge of the measured time-resolved fluorescence curve was reached if the fluorescence of the natural lens was included (Eq. (3); M6 to M9) [57].

The higher the number of free parameters, the higher was the required number of photons in the decay curve for the calculation of the fluorescence lifetime with a pre-determined error. For tri-exponential fitting of a fluorescence decay with an error of 10%, about 20,000 photons per pixel are necessary, but 400,000 photons per pixel are needed in a case of 4-exponential fit [12,59]. With the current FLIO device, such high photon counts cannot be measured in a practical way unless the spatial resolution is largely reduced.

5. Conclusion

In FLIO, the measured time-resolved autofluorescence of the eye originates from a layered structure. Despite the application of a confocal laser scanning technique, the fluorescence of the natural lens considerably influences the measured fluorescence signal of the FLIO device, especially in older patients with strong natural lens fluorescence. In all patients of this study, the mean fluorescence lifetime $\tau_{m,all}$ before cataract surgery was considerably longer than $\tau_{m,all}$ after the surgery because the implanted artificial lens emits no fluorescence signal. The impact of the natural lens was largest when applying a tri-exponential model, which utilizes the entire time range of the fluorescence signal. The application of a tri-exponential tailfit, which utilizes only the decay of the fluorescence signal, already reduces the influence of the natural lens. The mean fluorescence lifetime $\tau_{m,12}$ calculated from a tri-exponential tailfit in eyes with a natural lens corresponds very well with the pure fundus fluorescence lifetime $\tau_{m,all}$ of the same eyes after cataract surgery. The inclusion of a separate natural lens measurement in the fluorescence lifetime approximation yielded also good results, especially if high-quality natural lens measurements are used, but the achieved results cannot justify the extra effort and stress for the patient caused by the additional measurement of the natural lens. In contrast to Becker et al. [56], the results of the tri- or four-exponential fluorescence lifetime approximation using a temporal shift of the longest exponential component lead to inferior results compared to the tri-exponential tailfit for the utilized FLIO device. Thus, FLIO studies interested in investigating retinal physiology or pathology should use the mean fluorescence lifetime $\tau_{m,12}$ calculated from a tri-exponential tailfit instead of the currently used $\tau_{m,all}$ to minimize the influence of the natural lens on their analysis.

The best solution to suppress the natural lens fluorescence in FLIO data would be a modification of the FLIO hardware, e.g. by introducing an annular stop into the detection light path [40] or the separate measurement of the natural lens fluorescence from a non-excited location during the scanning process.

Funding

Thüringer Aufbaubank (2019 FGR 0083); Deutsche Forschungsgemeinschaft; Technische Universität Ilmenau (Publication Fund).

Biomedical Optics EXPRESS

Acknowledgments

We acknowledge support for the Article Processing Charge by the Open Access Publication Fund of the Technische Universität Ilmenau.

Disclosures

The authors declare that there are no conflicts of interest related to this article.

See Supplement 1 for supporting content.

References

1. D. Schweitzer, A. Kolb, M. Hammer, and E. Thamm, "τ mapping of the autofluorescence of the human ocular fundus," in *EOS/SPIE/ELA European Biomedical Optics Week – EBiOS*, 2000), 79–89.
2. D. Schweitzer, M. Hammer, F. Schweitzer, R. Anders, T. Doebbecke, S. Schenke, E. R. Gaillard, and E. R. Gaillard, "In vivo measurement of time-resolved autofluorescence at the human fundus," J. Biomed. Opt. **9**(6), 1214–1222 (2004).
3. M. Klemm, A. Dietzel, J. Haueisen, E. Nagel, M. Hammer, and D. Schweitzer, "Repeatability of Autofluorescence Lifetime Imaging at the Human Fundus in Healthy Volunteers," Curr. Eye Res. **38**(7), 793–801 (2013).
4. C. Dysli, G. Quellec, M. Abegg, M. N. Menke, U. Wolf-Schnurrbusch, J. Kowal, J. Blatz, O. La Schiazza, A. B. Leichtle, S. Wolf, and M. S. Zinkernagel, "Quantitative analysis of fluorescence lifetime measurements of the macula using the fluorescence lifetime imaging ophthalmoscope in healthy subjects," Invest. Ophthalmol. Visual Sci. **55**(4), 2106–2113 (2014).
5. S. Kwon, E. Borrelli, W. Fan, A. Ebraheem, K. M. Marion, and S. R. Sadda, "Repeatability of Fluorescence Lifetime Imaging Ophthalmoscopy in Normal Subjects With Mydriasis," Trans. Vis. Sci. Tech. **8**(3), 15 (2019).
6. L. Marcu, P. M. W. French, and D. S. Elson, *Fluorescence LifetimeSpectroscopy and Imaging : Principles and Applications in Biomedical Diagnostics* (CRC Press/Taylor & Francis Group, 2014).
7. L. Sauer, D. Schweitzer, L. Ramm, R. Augsten, M. Hammer, and S. Peters, "Impact of Macular Pigment on Fundus Autofluorescence Lifetimes," Invest. Ophthalmol. Visual Sci. **56**(8), 4668–4679 (2015).
8. L. Sauer, K. M. Andersen, B. X. Li, R. H. Gensure, M. Hammer, and P. S. Bernstein, "Fluorescence Lifetime Imaging Ophthalmoscopy (FLIO) of Macular Pigment," Invest. Ophthalmol. Visual Sci. **59**(7), 3094–3103 (2018).
9. M. Klemm, L. Sauer, S. Klee, D. Link, S. Peters, M. Hammer, D. Schweitzer, and J. Haueisen, "Bleaching effects and fluorescence lifetime imaging ophthalmoscopy," Biomed. Opt. Express **10**(3), 1446–1461 (2019).
10. S. R. Sadda, E. Borrelli, W. Y. Fan, A. Ebraheem, K. M. Marion, and S. Kwon, "Impact of mydriasis in fluorescence lifetime imaging ophthalmoscopy," PLoS One **13**(12), e0209194 (2018).
11. D. Schweitzer, S. Schenke, M. Hammer, F. Schweitzer, S. Jentsch, E. Birckner, W. Becker, and A. Bergmann, "Towards metabolic mapping of the human retina," Microsc. Res. Tech. **70**(5), 410–419 (2007).
12. D. Schweitzer, "Autofluorescence diagnostics of ophthalmic diseases," in *Natural Biomarkers for Cellular Metabolism: Biology, Techniques, and Applications*, 1st ed., V. V. Heikal and A. A. Ghukasyan, eds. (CRC Press/Taylor & Francis Group, 2015), pp. 317–344.
13. S. Peters, M. Hammer, and D. Schweitzer, "Two-photon excited fluorescence microscopy application for ex vivo investigation of ocular fundus samples," Proc. SPIE **8086**, 808605 (2011).
14. D. Schweitzer, S. Jentsch, S. Schenke, M. Hammer, C. Biskup, and E. Gaillard, "*Spectral and Time-resolved Studies on Ocular Structures*," in *European Conferences on Biomedical Optics* (SPIE, 2007), Vol. 6628.
15. D. Schweitzer, S. Quick, S. Schenke, M. Klemm, S. Gehlert, M. Hammer, S. Jentsch, and J. Fischer, "Comparison of parameters of time-resolved autofluorescence between healthy subjects and patients suffering from early AMD," Ophthalmologe **106**(8), 714–722 (2009).
16. D. Schweitzer, S. Quick, M. Klemm, M. Hammer, S. Jentsch, and J. Dawczynski, "Time-resolved autofluorescence in retinal vascular occlusions," Ophthalmologe **107**(12), 1145–1152 (2010).
17. S. Jentsch, D. Schweitzer, K. U. Schmidtke, S. Peters, J. Dawczynski, K. J. Bar, and M. Hammer, "Retinal fluorescence lifetime imaging ophthalmoscopy measures depend on the severity of Alzheimer's disease," Acta Ophthalmol. **93**(4), e241–e247 (2015).
18. D. Schweitzer, L. Deutsch, M. Klemm, S. Jentsch, M. Hammer, S. Peters, J. Haueisen, U. A. Müller, and J. Dawczynski, "Fluorescence lifetime imaging ophthalmoscopy in type 2 diabetic patients who have no signs of diabetic retinopathy," J. Biomed. Opt. **20**(6), 061106 (2015).
19. J. Schmidt, S. Peters, L. Sauer, D. Schweitzer, M. Klemm, R. Augsten, N. Muller, and M. Hammer, "Fundus autofluorescence lifetimes are increased in non-proliferative diabetic retinopathy," Acta Ophthalmol. **95**(1), 33–40 (2017).

Biomedical Optics EXPRESS

20. L. Sauer, S. Peters, J. Schmidt, D. Schweitzer, M. Klemm, L. Ramm, R. Augsten, and M. Hammer, "Monitoring macular pigment changes in macular holes using fluorescence lifetime imaging ophthalmoscopy," Acta Ophthalmol. **95**(5), 481–492 (2017).
21. L. Sauer, M. Klemm, S. Peters, D. Schweitzer, J. Schmidt, L. Kreilkamp, L. Ramm, D. Meller, and M. Hammer, "Monitoring foveal sparing in geographic atrophy with fluorescence lifetime imaging ophthalmoscopy - a novel approach," Acta Ophthalmol. **96**(3), 257–266 (2018).
22. L. Sauer, R. H. Gensure, K. M. Andersen, L. Kreilkamp, G. S. Hageman, M. Hammer, and P. S. Bernstein, "Patterns of Fundus Autofluorescence Lifetimes In Eyes of Individuals With Nonexudative Age-Related Macular Degeneration," Invest. Ophthalmol. Visual Sci. **59**(4), AMD65–AMD77 (2018).
23. K. M. Andersen, L. Sauer, R. H. Gensure, M. Hammer, and P. S. Bernstein, "Characterization of Retinitis Pigmentosa Using Fluorescence Lifetime Imaging Ophthalmoscopy (FLIO)," Trans. Vis. Sci. Tech. **7**(3), 20 (2018).
24. L. Sauer, R. H. Gensure, M. Hammer, and P. S. Bernstein, "Fluorescence Lifetime Imaging Ophthalmoscopy: A Novel Way to Assess Macular Telangiectasia Type 2," Ophthalmol. Retina **2**(6), 587–598 (2018).
25. L. Sauer, C. B. Komanski, A. S. Vitale, E. D. Hansen, and P. S. Bernstein, "Fluorescence Lifetime Imaging Ophthalmoscopy (FLIO) in Eyes With Pigment Epithelial Detachments Due to Age-Related Macular Degeneration," Invest. Ophthalmol. Visual Sci. **60**(8), 3054–3063 (2019).
26. L. Sauer, A. S. Vitale, K. M. Andersen, B. Hart, and P. S. Bernstein, "Fluorescence Lifetime Imaging Ophthalmoscopy (Flio) Patterns in Clinically Unaffected Children of Macular Telangiectasia Type 2 (Mactel) Patients," Retina **40**(4), 695–704 (2020).
27. C. Dysli, S. Wolf, and M. S. Zinkernagel, "Fluorescence Lifetime Imaging in Retinal Artery Occlusion," Invest. Ophthalmol. Visual Sci. **56**(5), 3329–3336 (2015).
28. C. Dysli, S. Wolf, and M. S. Zinkernagel, "Autofluorescence Lifetimes in Geographic Atrophy in Patients With Age-Related Macular Degeneration," Invest. Ophthalmol. Visual Sci. **57**(6), 2479–2487 (2016).
29. C. Dysli, R. Fink, S. Wolf, and M. S. Zinkernagel, "Fluorescence Lifetimes of Drusen in Age-Related Macular Degeneration," Invest. Ophthalmol. Visual Sci. **58**(11), 4856–4862 (2017).
30. C. Dysli, L. Berger, S. Wolf, and M. S. Zinkernagel, "Fundus Autofluorescence Lifetimes and Central Serous Chorioretinopathy," Retina **37**(11), 2151–2161 (2017).
31. C. Dysli, K. Schurch, E. Pascal, S. Wolf, and M. S. Zinkernagel, "Fundus Autofluorescence Lifetime Patterns in Retinitis Pigmentosa," Invest. Ophthalmol. Visual Sci. **59**(5), 1769–1778 (2018).
32. C. Dysli, S. Wolf, H. V. Tran, and M. S. Zinkernagel, "Autofluorescence Lifetimes in Patients With Choroideremia Identify Photoreceptors in Areas With Retinal Pigment Epithelium Atrophy," Invest. Ophthalmol. Visual Sci. **57**(15), 6714–6721 (2016).
33. C. Dysli, S. Wolf, M. Y. Berezin, L. Sauer, M. Hammer, and M. S. Zinkernagel, "Fluorescence lifetime imaging ophthalmoscopy," Prog. Retinal Eye Res. **60**, 120–143 (2017).
34. L. Sauer, K. M. Andersen, C. Dysli, M. S. Zinkernagel, P. S. Bernstein, and M. Hammer, "Review of clinical approaches in fluorescence lifetime imaging ophthalmoscopy," J. Biomed. Opt. **23**(09), 1–20 (2018).
35. C. Dysli, M. Dysli, V. Enzmann, S. Wolf, and M. S. Zinkernagel, "Fluorescence Lifetime Imaging of the Ocular Fundus in Mice," Invest. Ophthalmol. Visual Sci. **55**(11), 7206–7215 (2014).
36. C. Dysli, M. Dysli, M. S. Zinkernagel, and V. Enzmann, "Effect of pharmacologically induced retinal degeneration on retinal autofluorescence lifetimes in mice," Exp. Eye Res. **153**, 178–185 (2016).
37. D. Schweitzer, M. Hammer, and F. Schweitzer, "Limits of the confocal laser-scanning technique in measurements of time-resolved autofluorescence of the eye-ground," Biomed. Tech. **50**(9), 263–267 (2005).
38. D. Schweitzer, "Ophthalmic applications of FLIM," in *Fluorescence Lifetime Spectroscopy and Imaging : Principles and Applications in Biomedical Diagnostics*, L. Marcu, P. M. W. French, and D. S. Elson, eds. (CRC Press/Taylor & Francis Group, 2014), pp. 423–447.
39. G. E. Eldred and M. L. Katz, "Fluorophores of the Human Retinal-Pigment Epithelium - Separation and Spectral Characterization," Exp. Eye Res. **47**(1), 71–86 (1988).
40. M. Klemm, J. Blum, D. Link, M. Hammer, J. Haueisen, and D. Schweitzer, "Combination of confocal principle and aperture stop separation improves suppression of crystalline lens fluorescence in an eye model," Biomed. Opt. Express **7**(9), 3198–3210 (2016).
41. B.-G. Wang, "[Multiphoton microscopy and laser nanosurgery of the cornea using near-infrared nanojoule femtosecond laser pulses]," Dissertation (University Hospital Jena, Jena, 2006).
42. J. J. Hunter, B. Masella, A. Dubra, R. Sharma, L. Yin, W. H. Merigan, G. Palczewska, K. Palczewski, and D. R. Williams, "Images of photoreceptors in living primate eyes using adaptive optics two-photon ophthalmoscopy," Biomed. Opt. Express **2**(1), 139–148 (2011).
43. J. Mavadia, J. F. Xi, Y. P. Chen, and X. D. Li, "An all-fiber-optic endoscopy platform for simultaneous OCT and fluorescence imaging," Biomed. Opt. Express **3**(11), 2851–2859 (2012).
44. J. Park, J. A. Jo, S. Shrestha, P. Pande, Q. J. Wan, and B. E. Applegate, "A dual-modality optical coherence tomography and fluorescence lifetime imaging microscopy system for simultaneous morphological and biochemical tissue characterization," Biomed. Opt. Express **1**(1), 186–200 (2010).
45. J. R. Lakowicz, *Principles of Fluorescence Spectroscopy*, 3rd ed. (Springer, 2006), p. 954.
46. W. Becker, *The bh TCPSC Handbook*, 8th ed. (Becker & Hickl GmbH, 2019), p. 954.

Biomedical Optics EXPRESS

47. D. Schweitzer, "Metabolic mapping," in *Medical Retina: Focus on Retinal Imaging (Essentials in Ophthalmology)*, F. G. Holz and R. F. Spaide, eds. (Springer, 2010), pp. 107–123.
48. Early Treatment Diabetic Retinopathy Study Research Group, "Grading diabetic retinopathy from stereoscopic color fundus photographs–an extension of the modified Airlie House classification. ETDRS report number 10," Ophthalmology **98**(5), 786–806 (1991).
49. S. S. Shapiro and M. B. Wilk, "An Analysis of Variance Test for Normality (Complete Samples)," Biometrika **52**(3-4), 591–611 (1965).
50. M. Klemm, D. Schweitzer, S. Peters, L. Sauer, M. Hammer, and J. Haueisen, "FLIMX: A Software Package to Determine and Analyze the Fluorescence Lifetime in Time-Resolved Fluorescence Data from the Human Eye," PLoS One **10**(7), e0131640 (2015).
51. H. Pau, J. Degen, and H. H. Schmidtke, "Different Regional Changes of Fluorescence-Spectra of Clear Human Lenses and Nuclear Cataracts," Graefe's Arch. Clin. Exp. Ophthalmol. **231**(11), 656–661 (1993).
52. D. Moher, S. Hopewell, K. F. Schulz, V. Montori, P. C. Gotzsche, P. J. Devereaux, D. Elbourne, M. Egger, and D. G. Altman, "CONSORT 2010 explanation and elaboration: updated guidelines for reporting parallel group randomised trials," BMJ **340**(mar23 1), c869 (2010).
53. D. Schweitzer, L. Deutsch, M. Klemm, S. Jentsch, M. Hammer, J. Dawczynski, and U. A. Mueller, "Detection Of Early Metabolic Alterations In Diabetes Mellitus By Time-resolved Fundus Autofluorescence (FLIM)," Invest. Ophthalmol. Visual Sci. **52**, 1753 (2011).
54. D. K. Karumanchi, E. R. Gaillard, and J. Dillon, "Early Diagnosis of Diabetes through the Eye," Photochem. Photobiol. **91**(6), 1497–1504 (2015).
55. D. Schweitzer, M. Klemm, M. Hammer, S. Jentsch, and F. Schweitzer, "Method for simultaneous detection of functionality and tomography," Clinical and Biomedical Spectroscopy **7368**, 736804 (2009).
56. W. Becker, A. Bergmann, and L. Sauer, "Shifted-Component Model Improves FLIO Data Analysis," (Becker & Hickl GmbH, Berlin, Germany, 2018).
57. D. Schweitzer and M. Hammer, "Fluorescence Lifetime Imaging in Ophthalmology," in *Advanced Time-Correlated Single Photon Counting Applications*, W. Becker, ed. (Springer International Publishing, 2015), pp. 509–540.
58. M. G. O. Grafe, A. Hoffmann, and C. Spielmann, "Ultrafast fluorescence spectroscopy for axial resolution of flurorophore distributions," Appl. Phys. B: Lasers Opt. **117**(3), 833–840 (2014).
59. M. Koellner and J. Wolfrum, "How Many Photons Are Necessary for Fluorescence-Lifetime Measurements," Chem. Phys. Lett. **200**(1-2), 199–204 (1992).